

Engineering monolayer 1T-MoS₂ into a bifunctional electro-catalyst via sonochemical doping of isolated transition metal atoms

Thomas H.M. Lau[†], Simson Wu[†], Ryuichi Kato[‡], Tai-Sing Wu^{||}, Jiří Kulhavy[†], Jiaying Mo[†], Jianwei Zheng[†], John S. Foord[†], Yun-Liang Soo^{||}, Kazu Suenaga[‡], Matthew T. Darby^{§*}, S.C. Edman Tsang^{†*}

[†]Department of Chemistry, University of Oxford, Oxford, OX1 3QR, United Kingdom

[‡]National Institute of Advanced Industrial Science and Technology (AIST), Central 5, 1-1-1 Higashi, Tsukuba, Ibaraki 305-8565, Japan

^{||}Department of Physics, National Tsing Hua University, Hsinchu, Taiwan

[§]Thomas Young Centre and Department of Chemical Engineering, University College London, London WC1E 7JE, United Kingdom

ABSTRACT: There has been an intense research to develop 2H-MoS₂ based catalysts to reduce or eliminate the use of Pt/C at higher metal loading for hydrogen evolution reaction (HER) in catalytic hydrolysis of water, which enables the capture of renewable energy sources as fuel and chemical. However, the study of its uncommon polymorph, 1T-MoS₂ and particularly the doping effect with transition metal (TM) is rather limited due to the instability of this phase. Here we report a simple ambient temperature modification method using sonication to dope the single layer 1T-MoS₂ with various TM precursors. It is found that 1T-MoS₂ is more superior than corresponding 2H-MoS₂ and the inclusion of 3 wt% Pt or Pd can also further enhance the HER activity. STEM-EELS and XAS show the active single TM atom doping on this surface is to account for the high activity. Kinetic and DFT analyses also illustrate that the metallic nature of 1T-MoS₂ greatly facilitates the first proton reduction step from water, rendering it non-rate limiting as contrast to that of 2H-MoS₂. The inclusion of TM single doper such as Pd, despite at low loading, can offer the dramatic acceleration on the rate limiting recombination of H to H₂. As a result, a bifunctional catalysis for HER over this tailored composite structure is demonstrated which outperforms most reported catalysts in this area.

KEYWORDS: molybdenum disulphide, single atom catalysis, electrocatalysis, two-dimensional catalyst, hydrogen production, platinum, palladium

1 Introduction:

Predominantly, commercially available catalysts for electrochemical hydrogen evolution reaction (HER) are Pt-based materials due to their superior intrinsic activity^{1,2}. Unfortunately, the scarcity and high cost of Pt has inevitably inhibited the large scale industrial production of hydrogen through HER. In order to find more cost-effective alternatives, significant effort has been exerted in attempt to minimise the amount of noble metals contained in HER catalysts. It is hoped that the next generation thereof, will consist primarily of cheaper, earth-abundant materials yet will not sacrifice the overall performance³⁻⁵. One such candidate material is the naturally occurring layered semiconductor, molybdenum disulphide (MoS₂). Exfoliation of bulk MoS₂ gives rise to two-dimensional (2D) nanosheets that are inorganic analogues of graphene. MoS₂ nanosheets are found to possess exciting electronic, optical and catalytic properties, often enhanced compared to that of the bulk natural form⁶⁻⁸.

The most stable and only naturally occurring polymorph of MoS₂ is the 2H phase, consisting of trigonal prismatic coordinated Mo atoms⁹. With regards to HER catalysis, it is widely accepted that the activity of 2H-MoS₂ is dominated by edge sites that are exposed to the reaction interface when the thickness of MoS₂ is reduced to nanoscale.^{10,11} A commonly used descriptor for the activity of HER catalysts

is the free energy of hydrogen adsorption (ΔG_{H^*}), which suggests that optimal activity will be achieved when each step in the HER process is thermo-neutral (i.e. $\Delta G_{H^*} = 0$ eV)¹². Notably, 2H-MoS₂ edge sites exhibit ΔG_{H^*} of +0.08 eV¹³ compared to 2.00 eV on the inert basal plane¹⁴ and are therefore more active for HER. Thus, many different strategies have been employed to increase the ratio of active edge sites as compared to inert basal sites, with the hope of improving the overall HER activity.¹⁵⁻¹⁷ However, the number of basal sites is far larger than edge sites especially a thinner slab of MoS₂ is presented. More recently it has been shown that the 2H-MoS₂ basal plane can be activated by generating S defects in the surface.¹⁸⁻²⁰ Indeed the generation of S vacancies on the 2H-MoS₂ basal plane significantly lowers ΔG_{H^*} compared the pristine surface from 2.00 eV to approximately 0.14 eV²¹, thereby enhancing the HER activity.²² Moreover, we have demonstrated previously that a number of single transition metal atom dopants (TM) can be successfully chemisorbed on the basal plane of monolayer 2H-MoS₂, which further lower the hydrogen adsorption free energy of the surrounding S sites and in turn enhance the HER activity.²³

Although both the density and the intrinsic activity of the active sites have vastly increased after the introduction of basal S defects, the overall HER activity of 2H-MoS₂ is still

limited by sluggish charge transfer kinetics due to the semi-conducting nature of the phase²⁴. Thus with an intrinsic bandgap of 1.9eV²⁵, 2H-MoS₂ nanosheets struggle to compete with other zero band gap materials such as graphene and 2D carbide in terms of electrocatalytic activities.^{26,27}

Unlike 2H-MoS₂ nanosheets, the octahedral 1T phase is found to be metallic.^{28,29} However, since the 1T phase is thermally metastable, it does not occur in any natural forms of MoS₂ although 1T-MoS₂ can be synthesised through chemical exfoliation of bulk 2H-MoS₂ using Li or K intercalation.³⁰ The modified electronic properties caused due to the structural change during phase conversion are evidenced by an enhanced electrical conductivity of around 10⁷ times for 1T-MoS₂ as compared to 2H-MoS₂.³¹ In conjunction with dramatically improved electrical conductivity, 1T-MoS₂ exhibits significantly enhanced catalytic activity towards HER.^{8,32} Indeed ΔG_{H^+} on the 1T phase is reported to be approximately 0.12 eV¹⁴ which is comparable to that on 2H-MoS₂ with extensive S vacancies, though 1T-MoS₂ exhibits superior HER activity due to a greater number of active basal sites. Interestingly, under HER conditions the 1T phase undergoes a slight distortion to a lower energy 1T' structure that is stabilised by hydrogen adsorption during catalysis (notably in the remainder of the manuscript we refer to both phases as "1T" and do not distinguish between the two)^{14,33-35}. *Ab initio* calculations elucidating the mechanism of HER on 1T-MoS₂ nanosheets reveal a low kinetic barrier of 0.16 eV for the Volmer step ($H^+_{(aq)} + e^- \rightarrow H^*$) indicating facile charge transfer through the catalyst. Higher barriers of 0.95 eV and between 1.19 to 1.41 eV are also reported for the Heyrovsky ($H^+_{(aq)} + H^* + e^- \rightarrow H_{2(g)}$) and Tafel ($2H^* \rightarrow H_{2(g)}$) steps, respectively.^{14,34} Thus, HER on 1T-MoS₂ is not rate limited by the Volmer step but by the formation of H_{2(g)}.

Despite an array of positive results from recent advances in MoS₂ based HER materials, the catalytic activity of pure 1T-MoS₂ is still not comparable to those of TM-N-doped graphene, one of the recent most promising alternative material to 20% Pt/C²⁷. Based on the current understanding of the HER mechanism³⁴, modifying 1T-MoS₂ based catalysts to enhance the HER activity must aim to further reduce the activation barrier for the Heyrovsky and/or Tafel steps in order to overcome the rate limiting H₂ formation kinetics. Unfortunately, as stated, 1T-MoS₂ is thermally metastable and can easily be reverted back to the thermodynamically stable 2H phase at around 92 °C⁶. This impedes structural modifications making this task somewhat difficult. While it is logical to assume that the same strategies for surface manipulation used on 2H-MoS₂ can be applied to 1T-MoS₂, most methods involve relatively vigorous reaction conditions, for example hydrothermal reactions inside an autoclave, that will compromise the integrity of the 1T phase.³⁶

Herein, we report a very simple yet effective ambient condition sonochemical-assisted reductive doping method to synthesise monolayer 1T-^SMoS₂ with single transition metal adatoms that are chemisorbed at the basal plane (TM-1T-^SMoS₂, TM = Fe, Ni, Co, Pt, Pd) in a wet chemistry setup. An ambient condition synthesis prevents reconstruction of the 1T monolayer to the 2H phase yet allows us to still gently modify the catalytic surface with interfacial dopant atoms by sonication in water/alcohol at room temperature. Using advanced analytical techniques including High-Resolution Scanning Transmission Electron Microscopy (HR-STEM) with High-Angle Annular Dark-Field (HAADF) imaging, X-ray Photoelectron Spectroscopy (XPS), X-ray Absorption

Near Edge Structure (XANES), and Extended X-ray Absorption Fine Structure Spectroscopy (EXAFS), we provide direct evidence to confirm a stable incorporation of single transition metal adatoms onto the basal plane of 1T-^SMoS₂.

We report that the resulting TM-1T-^SMoS₂ samples as electrochemical HER catalysts give an excellent performance, with Pd-1T-^SMoS₂ exhibiting activity that is comparable to the best reported alternative materials to Pt/C.^{27,37} Solid-State Proton Nuclear Magnetic Resonance spectroscopy (¹H-NMR) indicates that 1T-^SMoS₂ surface is extensively covered with hydrogen species after the HER catalysis. The kinetic Tafel and rate analyses suggest that TM-1T-^SMoS₂ clearly operate as bi-functional catalysts whereby proton reduction to adsorbed H readily occurs on the pristine 1T-^SMoS₂ before transferred to the isolated TM dopant atoms on basal sites where Tafel recombination occurs. For the most promising dopants (TM = Pt and Pd), we have elucidated the structure-activity relationship of TM-1T-^SMoS₂ catalysts using Density Functional Theory (DFT). Our calculations confer to the bifunctional catalysis and also reveal that isolated Pt and Pd atoms on the 1T-^SMoS₂ basal plane significantly lower the activation barrier for the HER compared to the undoped analogue. The work in this study demonstrates that with proper treatment at ambient conditions, single nanosheets of ^SMoS₂ can retain the metastable 1T structure upon anchoring single TM species to the basal plane and the resulting catalysts exhibit dramatically improved HER activity over other MoS₂ based materials.

2 Results and Discussion:

Structural Characterisation of Isolated TM atoms on 1T-^SMoS₂. Monolayer 1T-^SMoS₂ nanosheets were prepared by chemical exfoliation of bulk 2H-^SMoS₂ using BuLi intercalation³⁰. For the purpose of comparison with 20% Pt/C reference, we particularly focus on the synthesis and characterisation of Pt doped 1T-^SMoS₂. The 5 wt% Pt precursor was added into the solution of the dispersed 1T-^SMoS₂ with a prolonged mixing in a sonication bath under ambient conditions for 24 hours. The strong adsorption of Pt species allowed for the successful incorporation of isolated Pt adatoms (~3 wt%) onto the basal plane of 1T-^SMoS₂. In this section we discuss our analysis of the structural features of Pt-1T-^SMoS₂ where we have used advanced analytical techniques including HAADF-STEM, EELS combined with *ab initio* simulations using DFT, XPS, XANES and EXAFS. (Details of preparation, DFT calculations, and analyses are listed in Supporting Information S1.)

First, we performed HR-STEM with HAADF imaging of Pt-1T-^SMoS₂ and compared our result with DFT calculated structure (Figures S1-S3). Analysing the structure from imaging the catalytic surface, we note the presence of a main octahedral structure (stacking in the 1T layer produces the ABC structure) which can be attributed to a monolayer 1T-^SMoS₂ (Figure 1). Occasionally, we can see a number of S vacancies on the surface presumably due to its creation by the butyl-lithium treatment. Notably, our "1T" MoS₂ nanosheets do not appear to be in pure polymorph as it's not currently possible to synthesise pure and stable 1T-^SMoS₂ using wet chemistry methods; 1T accounts for approximately ca. 76 % by surface area with the remainder of 2H polymorph (Figure S2). This is consistent to the reported value in the literature³⁶. The bright spots that can be seen on the 1T-^SMoS₂ surface correspond to Pt dopant atoms from the EELS. Notably these high intensity features are

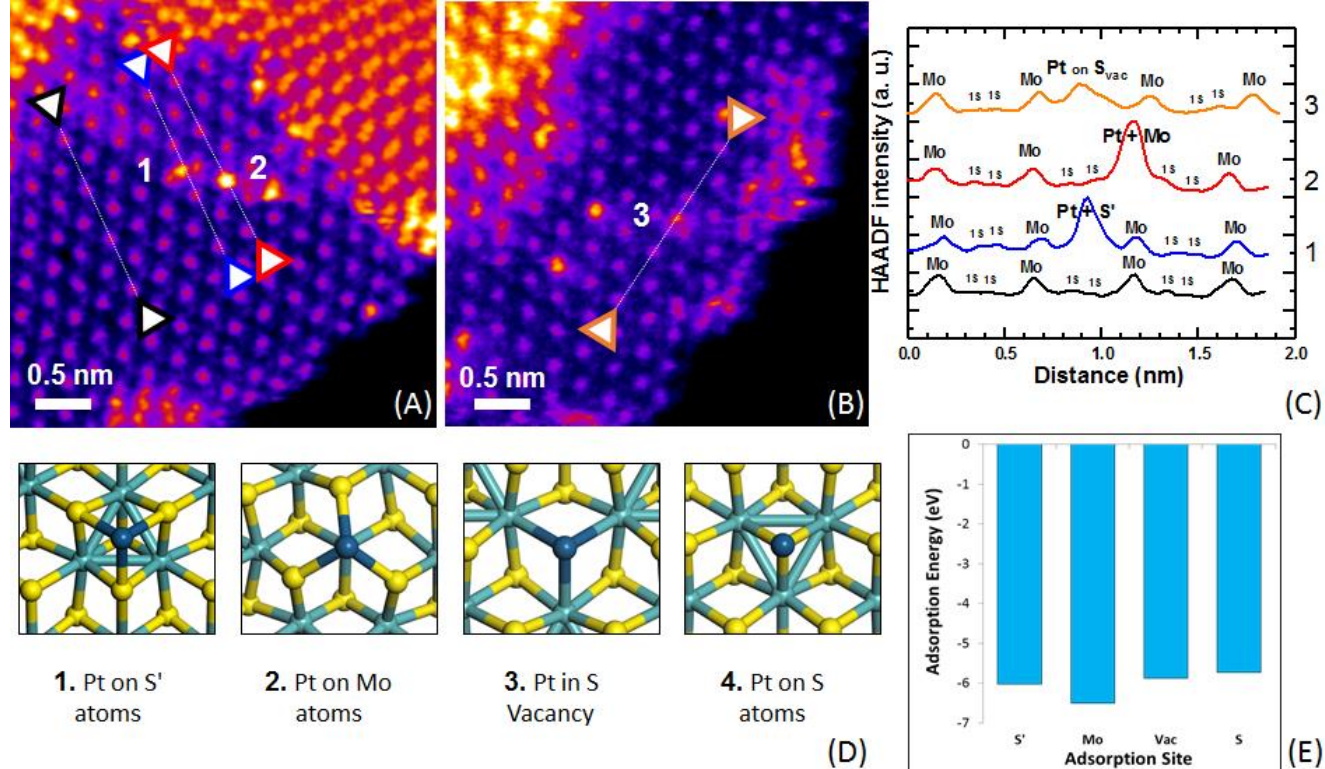


Figure 1. (a) and (b) HAADF-STEM of Pt-1T-^SMoS₂. (c) ADF intensity line profiles taken along the corresponding coloured line (Black, Blue, Red, and Orange) ($\langle 110 \rangle$ direction). (d) The simple representations of the Pt atom doping at position 1, 2 and 3 experimental observed on (A) and (B) and possibly at position 4. Side view models are included in supplementary information (Figure S4) (e) Adsorption Energy for Pt on each adsorption site.

isolated indicating the successful dispersion of single TM dopant atoms on the 1T basal plane. To further analyse the doping position of the transition metal atoms, intensity profiles of the ADF (Annular Dark-Field) image (Figure 1c) were taken in the $\langle 110 \rangle$ direction across the doped 1T-^SMoS₂ surfaces (Figure 1a and b), where paths connecting coloured triangles correspond to the equivalently coloured lines in the intensity profile. We provide peak assignments in Figure 1c with the black line being a control path where only Mo and S atoms are present. Along this line we detect four mid-intensity peaks corresponding to Mo atoms with each being separated by two low-intensity S peaks.

Considering paths 1, 2 and 3 (blue, red and orange, respectively) (Figure 1a and Figure 1b), we note a bright feature in each image which corresponds to a single atom of Pt. The appearance of the bright features give rise to three unique intensity profiles (Figure 1c) indicating that there are three different and stable doping sites for Pt on 1T-^SMoS₂. Considering path 1 (blue), the HAADF intensity profile shows that the Pt atom is located in the middle of two Mo atoms and two S atoms. Indeed, relaxation of such a structure using DFT gives the structure in panel 1 of Figure 1d which has an adsorption energy of Pt relative to a gas phase isolated atom of -6.02 eV, with the Pt atom positioned slightly offset from above the S atom in the lower S layer, which we label as S'. HAADF intensity path 2 (red) has a high-intensity peak coincident with a Mo atom and can therefore be attributed to the presence of a Pt atom on top of a Mo site. This configuration is the most frequently observed dopant position in our imaging samples and also has the most stable Pt adsorption energy calculated by DFT of -6.51 eV. According to the DFT calculated structure of this configuration, the Pt atom is bonded closely to three S atoms (2.22 Å) and slightly further from the underlying Mo atom (2.89 Å) which is in good agreement with our EXAFS results. Finally intensity profile 3 (orange) has a semi-bright feature and

corresponding mid-intensity peak off-centred between two Mo atoms (Figure 1c). The peak is not as intense as we find on profiles 1 or 2, though more intense than Mo or S atom. Thus, we attribute this to a Pt atom doped at an S Vacancy site (surface defect site). We calculated the DFT adsorption energy of Pt in an S vacancy to be -5.88 eV, showing the strength of binding on this site is comparable to Pt on the S' site. Our calculations also suggested that one final doping site is possible where Pt resides on the S top site, though a notably less stable heat of adsorption (-5.73 eV) precludes us from observing this experimentally (Figure 1d). A similar set of structural characterisations for Pd-1T-^SMoS₂ are presented in the Supporting Information (Figures S2-S3) and give similar conclusions for Pd doping, though DFT calculations indicate a stronger preference for Pd adsorption at the Mo top site and S' site. Overall, our STEM imaging results verified that we successfully dope isolated single metal atoms onto the 1T-^SMoS₂ basal plane without jeopardising the integrity of the 1T phase such that it may reconstruct to the more stable 2H phase.

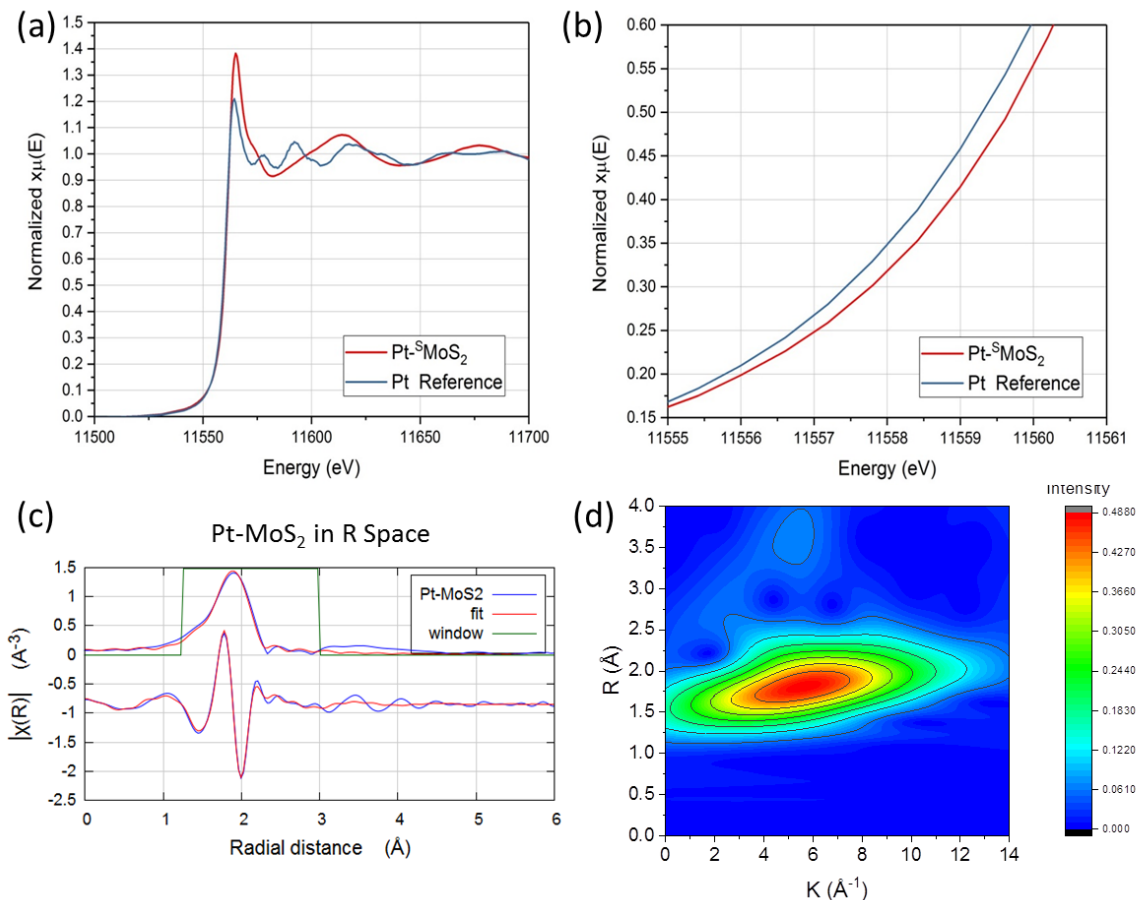


Figure 2. The Pt K-edge XANES spectra of Pt-1T- S-MoS_2 and the Pt (0) foil reference. (b) Enlarged version of A for the Pt K-edge region with energy range from 11555eV to 11561eV. (c) Fourier transforms of k^3 -weighted Pt K-edge of Extended X-ray absorption fine structure spectroscopy (EXAFS) spectra of Pt- S-MoS_2 and corresponding. (d) Morlet Wavelet transform analysis (Long Range) ($\text{Kappa} = 8$, $\text{Sigma} = 1$, $R = 0$ to 4 \AA).

XPS was used to analyse the surface composition of Pt dopants on Pt-1T- S-MoS_2 (Figure S5). We were able to detect the presence of isolated Pt on 1T- S-MoS_2 with a surface coverage of ca. 2.7% on the MoS_2 . This metal content is significantly lower than that of 20% Pt/C commonly used as the benchmark for HER (Table S1). Despite the use of room temperature, the Pt 4f XPS spectrum showed that most of the Pt are detected as metal Pt(0) or Pt^{2+} ions, which indicates that Pt(0) atoms were radically reduced from its HPtCl_4 precursor and dispersed onto the basal surface during the high energetic sonication process. As seen from Figure 2, the chemical environment of single Pt atoms dispersed on the 1T- S-MoS_2 surface is also analysed by XANES and EXAFS. The XANES curves (Figure 2a and Figure 2b) show that the Pt K-edge absorption positions of Pt-1T- S-MoS_2 are quite similar to that of Pt(0) foil, which once again confirms the presence of Pt(0) species. A first shell of Pt-S contribution {Bond length (\AA) = 2.31 ± 0.01 , Coordination number = 4.2 ± 0.2 , Energy difference (eV) = 7.4, Debye-Waller Factor = 0.006 ± 0.001 } is derived from Figure 2c. The absence of Pt-Pt interaction indicates that most Pt species on the basal plane of MoS_2 are not metal clusters or nanoparticles but rather single atoms or ions. This agrees with the STEM-EELS results shown in Figure 1. No strong Pt-Mo contribution can be found according to the fitting. This indicates that Pt is not strongly bound to Mo at the lattice but rather to the neighbouring S atoms. This is

similar with our previous findings on the chemical environment of transition metal dopants on 2H- S-MoS_2 basal sites²³. We also conducted the Wavelet transform (WT) analysis to separate backscattering atoms and provide a higher distance resolution and the resolution in the K-space of Pt K-edge (Figure 2d and Figure S6 for high resolution WT analysis). Only one WT intensity maximum at around 3.75 to 7.5 \AA^{-1} arising from the light atom coordinator can be well resolved from 0 to 4.0 \AA . whereas the intensity maximum associated with the Pt-Pt coordination at 8.5 \AA^{-1} cannot be detected for Pt-1T- S-MoS_2 . This once again reinforces the evidence that metallic Pt-Pt clusters are absent on the surface.

Electrocatalytic Performance and Tafel Analysis for HER. An electrochemical screening test using linear sweep voltammogram (LSV) for HER was conducted with five different transition metal elements (TM= Fe, Ni, Co, Pt, Pd) chosen as dopant atoms on 1T- S-MoS_2 using the same preparation method (Figure S7a). Figure 3a shows that Pd-1T- S-MoS_2 and Pt-1T- S-MoS_2 exhibit onset potentials (at a current density of -10 mA/cm^2) of approximately -140 mV and -223 mV , respectively, which is much smaller than that of the pristine 1T- S-MoS_2 (-300 mV). This suggests that the incorporation of single Pd and Pt atoms at 3 wt% with such simple doping technique can successfully increase the HER performance significantly as compared to undoped 1T- S-MoS_2 .

As far as we are aware the range of these onset potentials TM-1T- SMoS_2 is comparable to those of TM-N-doped graphene, the most promising alternative to Pt/C.²⁷ Moreover, we also compare the LSV results to that of the 2H phase and show that Pd-1T- SMoS_2 has an onset potential that is 200 mV smaller than that of Pd-2H- SMoS_2 ; this comes as no surprise since pristine 2H- SMoS_2 is a semiconductor and therefore exhibits poor charge transport that inhibits HER performance (Figure 3b). We also examine the durability of Pd-1T- SMoS_2 for HER using cyclic voltammetry. We show there is a marginal increase in onset potential of 10mV after 1000 cyclic voltammetry cycles. This confirms that the single transition metal atoms are firmly attached on the surface and the 1T phase doesn't convert back to 2H phase during the electrochemical reaction. (Figure 3c).

We then performed Tafel analysis to study the electrochemical kinetics of the HER as catalysed by each TM-1T- SMoS_2 sample (Figure 3d) and compared that with results from 2H- SMoS_2 as well as 20 % Pt/C. Measurements and analysis using the reference 20% Pt/C catalyst gave a Tafel slope of 33 mV/dec, which is similar previous results obtained elsewhere.^{37,38} At low overpotential, it is widely accepted that a Tafel slope of 30 mV/dec is indicative of HER that proceeds via the Tafel pathway. This mechanism depicts the readily reduction of H^+ on the metal surface giving a high coverage of H. Thus, the rate for HER is limited by H-H recombination to form H_2 .³⁷ In contrast, we have found that 2H- SMoS_2

reduction step before sufficiently H surface coverage for recombination is achieved. From the results of Tafel analysis on TM-1T- SMoS_2 (Figure 3d), Pd-1T- SMoS_2 and Pt-1T- SMoS_2 have Tafel slopes of 50 and 57 mV/dec, respectively which are slightly smaller compared to that of pristine 1T- SMoS_2 (61 mV/dec). Given the ca. 24% inclusion of 1T- SMoS_2 with 2H- SMoS_2 as shown in Figure S2, it is clear that the rate limiting for H_2 formation over the 1T- SMoS_2 based catalysts is likely to be on the Tafel step and the presence of TM can further reduce this kinetic barrier.

HER Mechanism of 1T- SMoS_2 . In order to assure that the 1T- SMoS_2 does not suffer from the limited H on its surface as that of 2H- SMoS_2 we have measured the H coverage over dried 1T- SMoS_2 quenched after HER catalysis. As shown from Figure S8, the strong but broad signal of ^1H indicative higher H coverage of 1T- SMoS_2 can be clearly seen. Simulation suggests that majority of this signal comes from ^1H on different S sites with different H attachments, which confers the higher H coverage on this surface. (Table S2) Since the rate determining step is likely to be on recombination of H to H_2 where high surface H at the equilibrium with H^+ from the solution is established. As a result, steady state approximation is employed to analyse the kinetic parameters of the HER over the 1T- SMoS_2 . The overall rate law indeed shows that the production rate of hydrogen shows a linear relationship with $[\text{H}^+]$ concentration within experimental error (Figure S9, Equation S1).

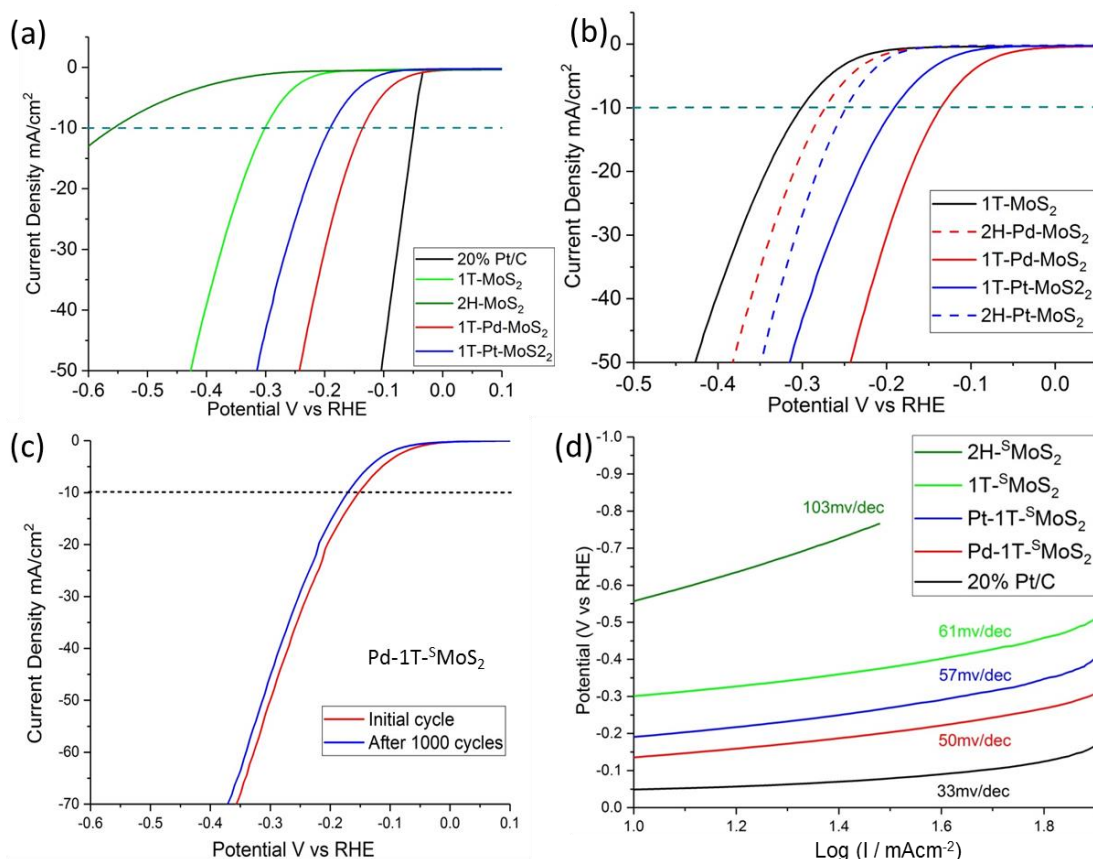


Figure 3. (a) LSV of Pd-1T- SMoS_2 , Pt-1T- SMoS_2 , 1T- SMoS_2 and 2H- SMoS_2 nanosheets and the reference 20% Pt/C in 0.5M H_2SO_4 at a scan rate of 50 mVs⁻¹. (b) LSV of 1T-Pd- SMoS_2 , 2H-Pd- SMoS_2 (c) Stability measurement of Pd-1T- SMoS_2 for HER, before and after 1000 cycles. (d) Tafel Analysis of Pt-1T- SMoS_2 and Pd-1T- SMoS_2

gives a Tafel slope of 103 mV/dec, indicating that the kinetics for H_2 formation is limited by the first Volmer proton re-

In additional, a series of Density Functional Theory (DFT) calculations has been performed. Using DFT, as per the

setup outlined in the Computational Setup section of the supporting information, we study the adsorption and recombination of H adatoms on $1T\text{-}^{\text{S}}\text{MoS}_2$ as well as that when the surface is doped with single atoms of Pt and Pd. Our calculations are performed on the distorted $1T\text{-}^{\text{S}}\text{MoS}_2$ monolayer that is a dynamically stable 2×1 reconstruction of $1T\text{-}^{\text{S}}\text{MoS}_2$. The $1T$ phase is destabilised by H^* adsorption and as a result exists as $1T'$ under HER conditions^{14,33–35} (Figure S10). The morphology of the $1T'$ surface results in two distinct S adsorption sites that are tensile or compressive strained as a result of Mo-Mo clustering in the reconstruction. Note that in our discussion we do not explicitly distinguish the two phases here though use “ $1T$ ” to refer to both. We also note that we do not explicitly account for the aqueous solvent in our calculations due to significant computational cost, though instead perform gas phase simulations with H/H_2 only. These calculations will allow us to compute free energies of adsorption with respect to $\text{H}_2(\text{g})$ as well as the Tafel barrier though cannot be used to quantify the barrier for the Volmer or Heyrovsky steps due to artificially introducing changes in the electrostatic potential along the reaction coordinates of these steps. However, given our experimental Tafel analysis suggests that the rate limiting step for HER on $\text{TM}\text{-}1T\text{-}^{\text{S}}\text{MoS}_2$ is the recombinative desorption of $\text{H}_2(\text{g})$, our calculations should be sufficient to draw some useful conclusions.

Considering the adsorption of H^* on pure $1T$, we find the most stable adsorption to be on an a tensile-strained S atom top site where $\Delta G(\text{H}^*)$ is $+0.14$ eV (Figure S14d); this compares well with values reported elsewhere³⁴. This value is significantly lower than those reported over 2H structure. Thus our calculations suggest that the adsorption of H^* on $1T\text{-}^{\text{S}}\text{MoS}_2$ is close to thermoneutral and significantly more so than $2\text{H}\text{-}^{\text{S}}\text{MoS}_2$, hence the superior HER activity of the former. Co-adsorption of two H^* adatoms on adjacent tensile-strained S atoms serves as the initial state for the Tafel H-H recombination step (Figure 4). The total free energy of adsorption for two H^* adatoms in this configuration is 0.48 eV, corresponding to a 0.20 eV repulsive interaction to overcome from having 2 H^* adatoms at infinite separation. The activation barrier to form $\text{H}_2(\text{g})$ from this initial state is 1.15 eV (or 1.35 eV from infinite separation), with the reaction from infinite separation being near ergodic. This barrier is in good agreement with that computed previously by others and is sufficiently large to inhibit fast recombinative kinetics³⁴. This further corroborates our suppositions based on our experimental Tafel and kinetic analyses.

HER Mechanism of $\text{TM}\text{-}1T\text{-}^{\text{S}}\text{MoS}_2$. Turning attention to the Pt and Pd-doped $1T\text{-}^{\text{S}}\text{MoS}_2$ basal plane, we consider both the undistorted and distorted surfaces. In our HAADF-STEM imaging, it is clear to see that the pure surface has hexagonal symmetry and is therefore corresponding to the undistorted $1T\text{-}^{\text{S}}\text{MoS}_2$ (Figure S2). However, it may be converted to distorted $1T\text{-}^{\text{S}}\text{MoS}_2$ upon the metal doping. Interestingly upon reconstruction of the $1T\text{-}^{\text{S}}\text{MoS}_2$ monolayer, both Pt and Pd can interact to the underneath Mo site (TM bonding to Mo on the second layer) with attempts to relax these atoms at other high symmetry sites (e.g. S top and S') resulting in displacement back to a Mo site. The reduction in surface symmetry of the $1T\text{-}^{\text{S}}\text{MoS}_2$ phase up H^* induced distortion gives rise to two different Mo top sites depending whether the TM is bound to one compressive-strained S atom and two tensile-strained S atoms (Mo top site 1) or two compressive-strained S atoms and one tensile-strained S atom (Mo top site 2) (Figure S12 and Figure S13). For

both Pt and Pd adsorption, the binding is notably stronger on Mo top site 1 whereby two bonds are formed with tensile-strained S atoms and one with the compressive-strained S atom.

Using the most stable Pt- and Pd-doped $1T\text{-}^{\text{S}}\text{MoS}_2$ surfaces (Mo top site 1), we computed the free energy of adsorption for H^* on various sites types as well as the minimum energy pathway for Tafel H-H recombination thereon. Our calculated adsorption energies show that the most stable site for H^* binding proximal to TM on $\text{TM}\text{-}1T\text{-}^{\text{S}}\text{MoS}_2$ is directly adsorbed to the Pt or Pd atom, with the H atom tilted away from the TM and between two tensile-strained S atoms (Figure S12b and Figure S12c). The $\Delta G(\text{H}^*)$ for this configuration on Pt- and Pd-doped $1T\text{-}^{\text{S}}\text{MoS}_2$ are -0.20 eV and $+0.49$ eV, respectively. (Figure S14) We were surprised to find that H^* adsorption to the transition metal dopant atoms is less thermoneutral than the corresponding value calculated for the undoped $1T\text{-}^{\text{S}}\text{MoS}_2$ monolayer ($+0.14$ eV), despite these materials exhibiting superior HER activity. Our work on transition metal doped $2\text{H}\text{-}^{\text{S}}\text{MoS}_2$, as well as similar findings from others, have suggested that S atoms proximal to TM become activated for HER thanks to more thermoneutral H^* adsorption.^{23,36} However, our calculations show that S atoms proximal to the Pt and Pd dopant bind H^* less strongly with $\Delta G(\text{H}^*)$ of $+0.69$ eV and $+0.68$ eV, respectively; in both cases the adsorption of H^* is less stable and notably further from thermoneutrality than that directly at the dopant site.

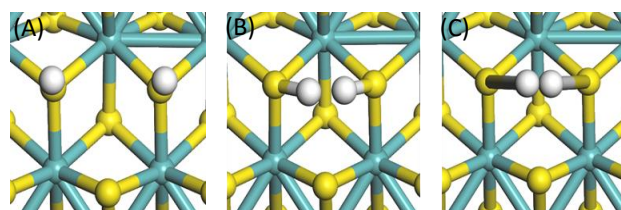


Figure 4. (a) Initial state (b) transition State (c) final State of Tafel recombination step

To further explore this inconsistency, we compute the Tafel barriers for recombinative H_2 desorption from $\text{TM}\text{-}1T\text{-}^{\text{S}}\text{MoS}_2$ (Figure S15). As with the pure $1T\text{-}^{\text{S}}\text{MoS}_2$ surface we first consider the most stable configuration for the co-adsorption of two H atoms proximal to the transition metal dopants. In both cases this configuration has both H directly bound to the Pt or Pd, though the binding configurations are different depending on the TM. On Pt dopant atoms, the co-adsorption is as two dissociated H adatoms whereas on Pd the adsorption is molecular. Interestingly, we find no molecular state on the former and no dissociated state on the latter. The $\Delta G(\text{H}^*)$ for the co-adsorbed configurations on Pt- and Pd-doped $1T\text{-}^{\text{S}}\text{MoS}_2$ are -0.39 eV and $+0.17$ eV, respectively. Our calculations show that on both TM-doped $1T\text{-}^{\text{S}}\text{MoS}_2$ surfaces the adsorption of $\text{H}_2(\text{g})$ is non-activated, thereby making the barrier for $\text{H}_2(\text{g})$ evolution via the Tafel mechanism equivalent to the negative of the adsorption energy for 2 H^* . Thus, the activation energy for the Tafel step is lowered from 1.15 eV on undoped $1T\text{-}^{\text{S}}\text{MoS}_2$ to 0.89 eV and 0.33 eV on Pt- and Pd-doped $1T\text{-}^{\text{S}}\text{MoS}_2$, respectively (Figure S15). The relative ordering of these activation barriers is in line with the HER activities we recorded in experiment.

Based on these insights from DFT calculations, we pose that the single dopant atoms are not solely responsible for

observed HER activity of TM-1T-^SMoS₂. If this were the case, we would expect near thermoneutral adsorption of H* or at least values of ΔG(H*) that are closer to zero than that for pure 1T-^SMoS₂. However in our case, the endothermic and weak adsorption of H* (ΔG(H*) = +0.49 eV) on the dopant atom in Pd-1T-^SMoS₂ suggests that H⁺ reduction via the Volmer step will be unfavourable and slow at this site, when in fact we observe the opposite; our experimental Tafel analysis demonstrates this catalyst is not limited by Volmer kinetics, but rather by H_{2(g)} desorption. Given the low coverage of Pd dopant atoms, the largest portions of the catalytic surface remain as undoped 1T-^SMoS₂ and are therefore still able to perform facile H⁺ reduction. Based on our HAADF-STEM imaging there appears to be a negligible effect to the structure and scattering intensity of Mo as close as first nearest neighbour to the dopant atoms. Thus, if we assume that modifications to the surface chemistry far from the dopant atoms are also negligible, a vast number of pristine 1T-^SMoS₂ sites will remain highly active for the Volmer step given a low kinetic barrier of 0.16 eV.³⁴

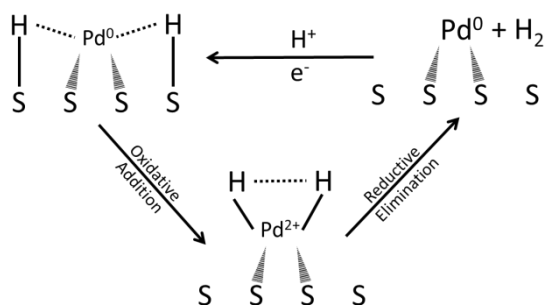


Figure 5. Schematic to summarise bifunctional catalysis over single Pd atom on 1T-^SMoS₂

The facile uptake of H⁺ from the aqueous phase will allow for well-maintained high H coverage across the 1T surface as we have observed experimentally. In fact previous studies of pure 1T phase have suggested the H* coverage at equilibrium to be between 25 and 35%.³⁵ A well-established equilibrium coverage in conjunction with high mobility of H* on the surface will facilitate diffusion into the Pd site. Notably such a diffusion of a single H* is endothermic by 0.35 eV, however at higher coverage diffusion into an already occupied Pd site to form the co-adsorbed Tafel step initial state from that on pure 1T-^SMoS₂ is highly favourable and exothermic by 0.31 eV. Thus, diffusion across the surface will allow H* to be shuttled from regions of pristine 1T-^SMoS₂ to the well-dispersed Pd dopant sites (Oxidative Addition) where the latter can facilitate H-H recombination via the Tafel step (Reductive Elimination) and therefore the composite single TM doped catalyst clearly operates bi-functionally (Figure 5). This mechanistic cycle ultimately accounts for the detection of both Pd⁰ and Pd²⁺ species in our X-ray analyses. Notably, we do not explore the possibility of the dopant atom facilitating the Heyrovsky step as this would require explicit modelling of the interfacial solvent, however it remains entirely possible that these single atoms also lower the Heyrovsky barrier as well as the Tafel barrier, though in either case the catalyst will be bi-functional.

3 Conclusions:

In conclusion, we have provided the first direct experimental evidence that single transition metal atoms such as Pd and

Pt can be chemically attached to the S sites of basal plane of the n-butyl lithium exfoliated 1T-^SMoS₂ by a mild radical assisted reduction of metal precursors using sonication in water/isopropanol at room temperature. The HAADF-STEM images, EELS mapping and XAS analyses suggest that there is no significant change to the crystallographic parameters of the underneath allurgically unstable monolayer 1T-^SMoS₂ polymorph; hence no conversion to 2-H phase upon the metal doping is reassured. Despite the low metal doping content their measured HER activity is shown to be far superior than corresponding 2-H ^SMoS₂; no significant deactivation is observed for 1000 catalytic cycles. High hydrogen coverage at steady state is maintained on this metallic 1-T surface during the HER as revealed by ¹H NMR and kinetic analysis. Tafel slope analysis and DFT modelling suggest the first proton reduction step from water on this surface is greatly facilitated, hence rendering the Volmer step non-rate limiting as contrast to that of 2-H ^SMoS₂. The inclusion of single Pd doper can also offer the dramatic acceleration on the rate limiting recombination of H to H₂. As a result, a bifunctional catalysis for HER over this tailored composite structure is demonstrated which outperforms most reported catalysts in this area. As shown from the DFT calculations, both the geometric and electronic factors exerted by the single TM dopants are therefore important parameters in further tuning the 2D 1T-^SMoS₂ structure for rational design of the composite materials as an efficient bifunctional electrocatalyst with immense potential for various electrochemical applications in the energy industries.

ASSOCIATED CONTENT

The Supporting Information is available free of charge on the ACS Publications website at DOI:

Experimental section including details of catalyst synthesis, technical details of catalysis analyses and calculations, various DFT calculations and modellings, TEM and STEM images, XPS spectra, WT analysis, HER tests, ¹H-SSNMR spectrum, steady state approximation on HER, AFM tests, schematic of HER, estimate of oxidation states by XANES.

AUTHOR INFORMATION

Corresponding Author

edman.tsang@chem.ox.ac.uk and
matthew.darby@ucl.ac.uk

Notes

The authors declare no competing financial interest.

ACKNOWLEDGMENT

The financial support of this project from the EPSRC research council of UK is acknowledged. The authors wish to thank the National Synchrotron Radiation Center, Hsinchu, Taiwan for accessing EXAFS facilities. RK and KS acknowledge the JSPS KAKENHI (JP16H06333) for support. M. T. D. is supported by the EPSRC Doctoral Prize Fellowship, grant reference number EP/N509577/1. The authors acknowledge the use of the UCL High Performance Computing Facilities (Legion@UCL, Grace@UCL and Thomas@UCL), and associated support services, in the completion of the computational part of this work. We are grateful to the UK Materials and Molecular Modelling Hub

for computational resources, which is partially funded by EPSRC (EP/P020194/1).

REFERENCES

- (1) Rausch, B.; Symes, M. D.; Chisholm, G.; Cronin, L. Decoupled Catalytic Hydrogen Evolution from a Molecular Metal Oxide Redox Mediator in Water Splitting. *2014*, 345 (6202), 2–7.
- (2) Fokas, A.; Kibble, T. W. B.; Grigoriou, A.; Zegarinski, B. Enhancing Hydrogen Evolution Activity in Water Splitting by Tailoring Li+-Ni(OH)2-Pt Interfaces. *2011*, No. December, 1256–1261.
- (3) McKone, J. R.; Marinescu, S. C.; Brunschwig, B. S.; Winkler, J. R.; Gray, H. B. Earth-Abundant Hydrogen Evolution Electrocatalysts. *Chem. Sci.* **2014**, 5 (3), 865–878. <https://doi.org/10.1039/c3sc51711j>.
- (4) Thoi, V. S.; Sun, Y.; Long, J. R.; Chang, C. J. Complexes of Earth-Abundant Metals for Catalytic Electrochemical Hydrogen Generation under Aqueous Conditions. *Chem. Soc. Rev.* **2013**, 42 (6), 2388–2400. <https://doi.org/10.1039/c2cs35272a>.
- (5) Roger, I.; Shipman, M. A.; Symes, M. D. Earth-Abundant Catalysts for Electrochemical and Photoelectrochemical Water Splitting. *Nature Reviews Chemistry*. Nature Publishing Group January 11, 2017. <https://doi.org/10.1038/s41570-016-0003>.
- (6) Wypych, F.; Schollhorn, R. 1T-MoS₂, a New Metallic Modification of Molybdenum Disulfide. *J. CHEM. SOC. CHEM. COMMUN.* **1992**, No. 1386, 1386–1388.
- (7) Singh, N.; Jabbour, G.; Schwingenschlöggl, U. Optical and Photocatalytic Properties of Two-Dimensional MoS₂. *Eur. Phys. J. B* **2012**, 85 (11), 392. <https://doi.org/10.1140/epjb/e2012-30449-7>.
- (8) Voiry, D.; Salehi, M.; Silva, R.; Fujita, T.; Chen, M.; Asefa, T.; Shenoy, V. B.; Eda, G.; Chhowalla, M. Conducting MoS₂ Nanosheets as Catalysts for Hydrogen Evolution Reaction. *Nano Lett.* **2013**, 13 (12), 6222–6227. <https://doi.org/10.1021/nl403661s>.
- (9) Liang, K. S.; Chianelli, R. R.; Chien, F. Z.; Moss, S. C. The Term “Poorly Crystalline,” Used Here to Describe Our Samples, Is Not. *J. Non-Crystalline Solids* **1986**, 79, 251–273.
- (10) Hinnemann, B.; Moses, P. G.; Bonde, J.; Jørgensen, K. P.; Nielsen, J. H.; Hørch, S.; Chorkendorff, I.; Nørskov, J. K. Biomimetic Hydrogen Evolution: MoS₂ Nanoparticles as Catalyst for Hydrogen Evolution. *J. Am. Chem. Soc.* **2005**, 127 (15), 5308–5309. <https://doi.org/10.1021/ja0504690>.
- (11) Jaramillo, T. F.; Jørgensen, K. P.; Bonde, J.; Nielsen, J. H.; Hørch, S.; Chorkendorff, I. Identification of Active Edge Sites for Electrochemical H₂ Evolution from MoS₂ Nanocatalysts. *Science* (80-.). **2007**, 317 (5834), 100 LP-102. <https://doi.org/10.1126/science.1141483>.
- (12) Nørskov, J. K.; Bligaard, T.; Logadottir, A.; Kitchin, J. R.; Chen, J. G.; Pandelov, S.; Stimming, U. Trends in the Exchange Current for Hydrogen Evolution. *J. Electrochem. Soc.* **2005**, 152 (3), J23. <https://doi.org/10.1149/1.1856988>.
- (13) Nanocatalysts, M.; Jaramillo, T. F.; Jørgensen, K. P.; Bonde, J.; Nielsen, J. H.; Hørch, S.; Chorkendorff, I. Identification of Active Edge Sites for Electrochemical H₂ Evolution From. **2007**, 317 (July), 100–103.
- (14) Tsai, C.; Chan, K.; Nørskov, J. K.; Abild-Pedersen, F. Theoretical Insights into the Hydrogen Evolution Activity of Layered Transition Metal Dichalcogenides. *Surf. Sci.* **2015**, 640, 133–140. <https://doi.org/10.1016/j.susc.2015.01.019>.
- (15) Kibsgaard, J.; Chen, Z.; Reinecke, B. N.; Jaramillo, T. F. Engineering the Surface Structure of MoS₂ to Preferentially Expose Active Edge Sites for Electrocatalysis. *Nat. Mater.* **2012**, 11 (11), 963–969. <https://doi.org/10.1038/nmat3439>.
- (16) Chung, D. Y.; Park, S. K.; Chung, Y. H.; Yu, S. H.; Lim, D. H.; Jung, N.; Ham, H. C.; Park, H. Y.; Piao, Y.; Yoo, S. J.; et al. Edge-Exposed MoS₂ Nano-Assembled Structures as Efficient Electrocatalysts for Hydrogen Evolution Reaction. *Nanoscale* **2014**, 6 (4), 2131–2136. <https://doi.org/10.1039/c3nr05228a>.
- (17) Hu, J.; Huang, B.; Zhang, C.; Wang, Z.; An, Y.; Zhou, D.; Lin, H.; Leung, M. K. H.; Yang, S. Engineering Stepped Edge Surface Structures of MoS₂ Sheet Stacks to Accelerate the Hydrogen Evolution Reaction. *Energy Environ. Sci.* **2017**, 10 (2), 593–603. <https://doi.org/10.1039/c6ee03629e>.
- (18) Li, H.; Tsai, C.; Koh, A. L.; Cai, L.; Contryman, A. W.; Fragapane, A. H.; Zhao, J.; Han, H. S.; Manoharan, H. C.; Abild-Pedersen, F.; et al. Activating and Optimizing MoS₂ Basal Planes for Hydrogen Evolution through the Formation of Strained Sulphur Vacancies. *Nat. Mater.* **2015**, 15 (1), 48–53. <https://doi.org/10.1038/nmat4465>.
- (19) Ye, G.; Gong, Y.; Lin, J.; Li, B.; He, Y.; Pantelides, S. T.; Zhou, W.; Vajtai, R.; Ajayan, P. M. Defects Engineered Monolayer MoS₂ for Improved Hydrogen Evolution Reaction. *Nano Lett.* **2016**, 16 (2), 1097–1103. <https://doi.org/10.1021/acs.nanolett.5b04331>.
- (20) Tsai, C.; Li, H.; Park, S.; Park, J.; Han, H. S.; Nørskov, J. K.; Zheng, X.; Abild-Pedersen, F. Electrochemical Generation of Sulfur Vacancies in the Basal Plane of MoS₂ for Hydrogen Evolution. *Nat. Commun.* **2017**, 8, 1–8. <https://doi.org/10.1038/ncomms15113>.
- (21) Wu, W.; Niu, C.; Wei, C.; Jia, Y.; Li, C.; Xu, Q. Activation of MoS₂ Basal Planes for Hydrogen Evolution through Zinc. *Angew. Chemie Int. Ed.* **2019**, 1–6. <https://doi.org/10.1002/anie.201812475>.
- (22) Xu, Y.; Wang, L.; Liu, X.; Zhang, S.; Liu, C.; Yan, D.; Zeng, Y.; Pei, Y.; Liu, Y.; Luo, S. Monolayer MoS₂ with S Vacancies from Interlayer Spacing Expanded Counterparts for Highly Efficient Electrochemical Hydrogen Production. *J. Mater. Chem. A* **2016**, 4 (42), 16524–16530. <https://doi.org/10.1039/C6TA06534A>.
- (23) Lau, T. H. M.; Lu, X.; Kulhavy, J.; Wu, S.; Lu, L.; Wu, T. S.; Kato, R.; Foord, J. S.; Soo, Y. L.; Suenaga, K.; et al. Transition Metal Atom Doping of the Basal Plane of MoS₂ Monolayer Nanosheets for Electrochemical Hydrogen Evolution. *Chem. Sci.* **2018**, 9 (21), 4769–4776. <https://doi.org/10.1039/c8sc01114a>.
- (24) Tsai, C.; Abild-pedersen, F. Tuning the MoS₂ Edge-Site Activity for Hydrogen Evolution via Support Interactions. **2014**. <https://doi.org/10.1021/nl404444k>.
- (25) Li, T.; Galli, G. Electronic Properties of MoS₂ Nanoparticles. *J. Phys. Chem. C* **2007**, 111 (44), 16192–16196. <https://doi.org/10.1021/jp075424v>.
- (26) Ito, Y.; Cong, W.; Fujita, T.; Tang, Z.; Chen, M. High Catalytic Activity of Nitrogen and Sulfur Co-Doped Nanoporous Graphene in the Hydrogen Evolution Reaction. *Angew. Chemie - Int. Ed.* **2015**, 54 (7), 2131–2136. <https://doi.org/10.1002/anie.201410050>.
- (27) Zhong, Y.; Xia, X. H.; Shi, F.; Zhan, Y.; Tu, J. P.; Fan, H. J. Transition Metal Carbides and Nitrides in Energy Storage and Conversion. *Adv. Sci.* **2015**, 3 (5). <https://doi.org/10.1002/advs.201500286>.
- (28) Ambrosi, A.; Sofer, Z.; Pumera, M. Lithium Intercalation Compound Dramatically Influences the Electrochemical Properties of Exfoliated MoS₂. *Small* **2015**, 11 (5), 605–612. <https://doi.org/10.1002/smll.201400401>.
- (29) Kappera, R.; Voiry, D.; Yalcin, S. E.; Branch, B.; Gupta, G.; Mohite, A. D.; Chhowalla, M. Phase-Engineered Low-Resistance Contacts for Ultrathin MoS₂ Transistors. *Nat. Mater.* **2014**, 13 (12), 1128–1134. <https://doi.org/10.1038/nmat4080>.
- (30) Splendiani, A.; Sun, L.; Zhang, Y.; Li, T.; Kim, J.; Chim, C. Y.; Galli, G.; Wang, F. Emerging Photoluminescence in Monolayer MoS₂. *Nano Lett.* **2010**, 10 (4), 1271–1275. <https://doi.org/10.1021/nl903868w>.
- (31) Acerce, M.; Voiry, D.; Chhowalla, M. Metallic 1T Phase MoS₂ Nanosheets as Supercapacitor Electrode Materials. *Nat. Nanotechnol.* **2015**, 10 (4), 313–318. <https://doi.org/10.1038/nnano.2015.40>.

- (32) Lukowski, M. A.; Daniel, A. S.; Meng, F.; Forticaux, A.; Li, L.; Jin, S. Enhanced Hydrogen Evolution Catalysis from Chemically Exfoliated Metallic MoS₂ Nanosheets. *J. Am. Chem. Soc.* **2013**, *135* (28), 10274–10277. <https://doi.org/10.1021/ja404523s>.
- (33) Putungan, D. B.; Lin, S.; Kuo, J. A First-Principles Examination of Conducting Reaction and Its Enhancement by Strain. *ACS Catal.* **2015**, *2*, 21702–21708. <https://doi.org/10.1039/c5cp03799a>.
- (34) Tang, Q.; Jiang, D. E. Mechanism of Hydrogen Evolution Reaction on 1T-MoS₂ from First Principles. *ACS Catal.* **2016**, *6* (8), 4953–4961. <https://doi.org/10.1021/acscatal.6b01211>.
- (35) Hu, T.; Li, R.; Dong, J. A New (2 × 1) Dimerized Structure of Monolayer 1T-Molybdenum Disulfide, Studied from First Principles Calculations. *J. Chem. Phys.* **2013**, *139* (17). <https://doi.org/10.1063/1.4827082>.
- (36) Liu, G.; Robertson, A. W.; Li, M. M.-J. J.; Kuo, W. C. H. H.; Darby, M. T.; Muhieddine, M. H.; Lin, Y.-C. C.; Suenaga, K.; Stamatakis, M.; Warner, J. H.; et al. MoS₂ Monolayer Catalyst Doped with Isolated Co Atoms for the Hydrodeoxygenation Reaction. *Nat. Chem.* **2017**, *9* (8), 810–816. <https://doi.org/10.1038/nchem.2740>.
- (37) Ding, Q.; Song, B.; Xu, P.; Jin, S. Efficient Electrocatalytic and Photoelectrochemical Hydrogen Generation Using MoS₂ and Related Compounds. *CHEMPR* **2016**, *1* (5), 699–726. <https://doi.org/10.1016/j.chempr.2016.10.007>.
- (38) Tavares, M. C.; Machado, S. A. S.; Mazo, L. H. Study of Hydrogen Evolution Reaction in Acid Medium on Pt Microelectrodes. *Electrochim. Acta* **2001**, *46* (28), 4359–4369. [https://doi.org/10.1016/S0013-4686\(01\)00726-5](https://doi.org/10.1016/S0013-4686(01)00726-5).

Table of Contents artwork

